

MR Elastography Sampling Requirements: Preliminary Investigations

K. J. Glaser¹, A. Manduca¹, and R. L. Ehman¹

¹Radiology, Mayo Clinic, Rochester, MN, United States

Introduction: Imaging the mechanical properties of tissue has emerged as an important topic in both the fields of ultrasonography and MRI. In MRI, phase-based methods, such as dynamic MR elastography (MRE, [1]) have been developed to image tissue response to extrinsic and intrinsic stresses. These images of tissue deformation are then processed [2] to determine material properties. Achieving accurate measurements of tissue properties can require the acquisition of 3D, full-vector displacement data at numerous time points, which can be prohibitive in clinical settings. One way to reduce acquisition times is to reduce the resolution of the acquisition matrix, particularly the number of phase-encoding lines in k-space. The challenge is to determine the minimum amount of k-space that must be sampled to produce acceptable assessments of tissue mechanical properties. The purpose of this work is to investigate some of the properties of MRE data that affect the minimum amount of k-space that must be acquired.

Theory: In MRE, multiple datasets are acquired with different time offsets between the motion and the motion-encoding gradients (MEG), as well as with different MEG directions to fully sample the vector motion and to perform phase-contrast calculations. Let the transverse magnetization for any one of these acquisitions be described by $p(\mathbf{r},t) = m(\mathbf{r}) \cdot \exp(i\phi(\mathbf{r},t))$, where $m(\mathbf{r})$ is the magnitude of the transverse magnetization (assumed to be time independent) and $\phi(\mathbf{r},t)$ is the phase. A result of applying a dynamic stress to tissue during MRE is to produce a shear wave field that propagates throughout the tissue. The MEG encode that shear wave field into the phase of the transverse magnetization. If the shear wave field is approximated as a simple plane wave, then the encoded dynamic phase data can be written as Eq. (1), where A is the amplitude of the phase variations due to the motion and MEG, λ is the wavelength of the wave propagating in the direction $\hat{\mathbf{n}}$ with a frequency F and arbitrary phase offset α . The transverse magnetization can then be written as Eq. (2), where $\phi_b(\mathbf{r})$ is a static background phase term that arises from such things as off resonance, concomitant fields, and gradient imperfections. The k-space for this transverse magnetization can be written as Eq. (3), where $\mathcal{F}\{\cdot\}$ is the spatial Fourier transform and \otimes is the convolution. The second exponential can be rewritten using the Jacobi-Anger expansion and the linearity of the Fourier transform to give Eq. (4), where $\mathcal{F}\{\dots\}$ represents the Fourier transform of the original static object and $J_n(A)$ is the Bessel function of the first kind of order n . The last Fourier transform in Eq. (4) can be written as $\delta(\mathbf{k} + n\hat{\mathbf{n}}/\lambda)$, where δ is the delta function, allowing Eq. (4) to be written as Eq. (5). This indicates that the effect of MRE motion encoding is to produce periodic replicas or ghosts of the k-space of the static object. These ghosts are separated in k-space by $1/\lambda$ and are weighted by $J_n(A)$. The required amount of k-space to be

measured will depend on both the wavelength of the shear waves as well as the phase amplitude A of the encoded waves. Sampling a finite amount of k-space results in a loss of some of this high-frequency k-space information, which produces inaccuracies in the image data. These errors are then compounded when images with two different MEG directions are combined to calculate the phase-difference images used in most MRE inversion algorithms.

Methods: Numerical simulations were performed in 1D to demonstrate this model of MRE k-space data, to determine the impact that undersampling k-space data has on the elastograms, and to determine the amount of k-space needed for stable inversions. Complex images with unit magnitude and sinusoidal phase with various amplitudes and wavelengths were constructed. Each case simulated a 20-cm FOV with a 60-Hz (F) wave discretized with $N_s=512$ pixels and 8 time offsets. The shear modulus of the material was purely real with $G \in [0.5, 10]$ kPa, and the phase amplitude for each sensitization direction was $A \in [0.5, 5]$ radians. For each combination of G and A , the 1D images representing the positive and negative motion-encoding data were created and Fourier transformed into k-space. Each k-space image was windowed with a N_w -point apodizing window of the form $(1-x^2)^2$, where $N_w \in [3, 511]$ and x contains N_w evenly spaced points from -1 to 1 [3]. The windowed k-space data were Fourier transformed back to image space and the phase difference of the two "motion-encoding" directions was calculated. The phase data were then processed like regular MRE data to obtain estimates of G with a direct inversion algorithm incorporating 3-point derivative kernels and no additional smoothing. The mean and standard deviation (SD) of G over the middle half of each image were calculated and recorded. To correlate the amount of k-space truncation with the error E in the stiffness estimates ($E \in [1, 50]\%$ difference from the true G), the largest window size that resulted in a mean G and a SD of G that deviated from the true G by more than E were noted and the next largest window size W_E was recorded for each G and A . Since the required amount of k-space was expected to increase with A and $1/\lambda$, for each value of E , the W_E versus A/λ data were fit to a line and the slope M of the line (in units of window size per rad/cm, or $\text{cm}^{-1}/(\text{rad}/\text{cm})$, or rad) was recorded. The M versus E data were then fit to an exponential to see how the choice of k-space size for a particular G and A affects the error in the estimates of G .

Results: Figure 1(a) shows an example 1D simulated phantom with $G = 2$ kPa and $A = 2$ radians. The k-space data have numerous peaks due to the ghosting effect in Eq. (5) (Fig. 1(b)). An example k-space windowing function is also shown in Fig. 1(b). Figure 1(c) shows the final elastogram for this truncated data. The reconstructed G has a mean of $(2.0183 \pm 0.2182) + (0.0002 \pm 0.1164)i$. Figure 2 (first column) shows a cumulative plot of what size k-space window is required to obtain 10% error in G (top row) or the SD of G (bottom row) for a particular A/λ . The second column shows the cumulative results from performing fits such as those in the first column for several different error percentages.

Discussion and Conclusions: These results support the fundamental hypothesis of this work that MRE data with high wave amplitudes in the phase data and short wavelengths require the acquisition of more k-space than would be necessary for the static object or even for low-amplitude motion or longer wavelengths. This can result in situations where the raw k-space data are not fully sampled, which can produce artifacts in the elastograms (e.g., Fig. 1(c)). The plots in Fig. 2 suggest that it may be possible to relate the amount of k-space truncation to the amount of error in the elastograms. Such a theory would be beneficial for optimizing MRE acquisition protocols by reducing the amount of k-space that has to be acquired. The results presented here may not directly port to conventional MRE acquisitions because the model is still very simple. For example, it does not account for more complicated magnitude and phase signal variations, noise, or discretization effects [4]. However, it may be possible to extend this model and methodology to include such behavior.

Bibliography: [1] Muthupillai R, Science 1995;269:1854-7. [2] Manduca A, Med Image Anal 2001;5(4):237-54. [3] Romano AJ, IEEE Trans Ultrason Ferroelect Freq Contr 2000;47(6):1575-81. [4] Papazoglou S, Phys Med Biol 2008;53(12):3147-58.

$$\begin{aligned} \varphi_d(\mathbf{r},t) &= A \cdot \sin(2\pi \cdot \hat{\mathbf{n}}/\lambda + 2\pi F t + \alpha) & (1) \\ p(\mathbf{r},t) &= m(\mathbf{r}) \cdot \exp[i \cdot [\varphi_b(\mathbf{r}) + A \cdot \sin(2\pi \cdot \hat{\mathbf{n}}/\lambda + 2\pi F t + \alpha)]] & (2) \\ P(\mathbf{k},t) &= \mathcal{F}\{m(\mathbf{r}) \cdot \exp[i \cdot \varphi_b(\mathbf{r})]\} \otimes \mathcal{F}\{\exp[i \cdot A \cdot \sin(2\pi \cdot \hat{\mathbf{n}}/\lambda + 2\pi F t + \alpha)]\} & (3) \\ P(\mathbf{k},t) &= \mathcal{F}\{\dots\} \otimes \sum_{n=-\infty}^{\infty} J_n(A) \cdot \exp[in(2\pi F t + \alpha)] \cdot \mathcal{F}\{\exp[2\pi i n \cdot \hat{\mathbf{n}}/\lambda]\} & (4) \\ P(\mathbf{k},t) &= \sum_{n=-\infty}^{\infty} J_n(A) \cdot \exp[in(2\pi F t + \alpha)] \cdot \left[\mathcal{F}\{\dots\} \otimes \delta(\mathbf{k} + \frac{n\hat{\mathbf{n}}}{\lambda}) \right] & (5) \end{aligned}$$

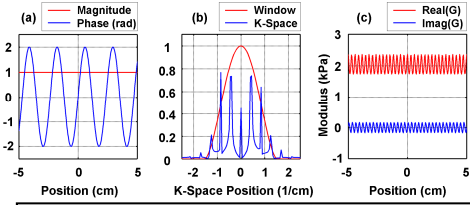


Figure 1: (a) Example of a simulated phantom. (b) K-space of phantom and an example apodizing window. (c) Reconstructed shear modulus.

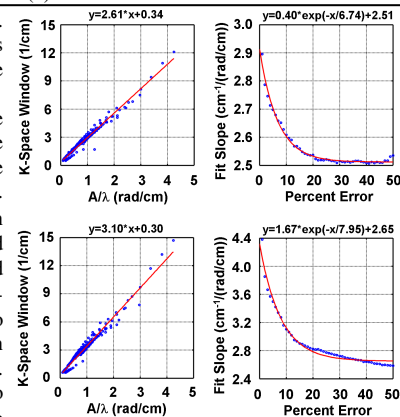


Figure 2: Left column are results targeting a 10% error in G . Right column are results indicating the amount of k-space required to achieve a specific error. The top and bottom rows use the error between the actual G and the mean of G or the SD of G , respectively.